

Torsion Balance Experiments Enable Direct Detection of Sub-eV Dark Matter

Shigeki Matsumoto,^{1,*} Jie Sheng,^{2,3,4,†} Chuan-Yang Xing,^{5,‡} and Lin Zhu^{6,§}

¹*Kavli IPMU (WPI), UTIAS, University of Tokyo, Kashiwa, 277-8583, Japan*

²*Tsung-Dao Lee Institute & School of Physics and Astronomy, Shanghai Jiao Tong University, China*

³*State Key Laboratory of Dark Matter Physics, Tsung-Dao Lee Institute & School of Physics and Astronomy, Shanghai Jiao Tong University, Shanghai 200240, China*

⁴*Key Laboratory for Particle Astrophysics and Cosmology (MOE) & Shanghai Key Laboratory for Particle Physics and Cosmology, Shanghai Jiao Tong University, Shanghai 200240, China*

⁵*College of Science, China University of Petroleum (East China), Qingdao 266580, China*

⁶*National Gravitation Laboratory, MOE Key Laboratory of Fundamental Physical Quantities Measurement & Hubei Key Laboratory of Gravitation and Quantum Physics, School of Physics, Huazhong University of Science and Technology, Wuhan 430074, People's Republic of China*

Light dark matter with sub-eV masses has a high number density in our galaxy, and its scattering cross section with macroscopic objects can be significantly enhanced by coherence effects. Repeated scattering with a target object can induce a measurable acceleration. Torsion balance experiments with geometric asymmetry are, in principle, capable of detecting such signals. Our analysis shows that existing torsion balances designed to test the Equivalence Principle already place the most stringent constraints on DM–nucleon scattering in the $(10^{-2}, 1)$ eV mass range.

INTRODUCTION

Numerous astronomical and cosmological observations have confirmed the existence of dark matter (DM) [1], which accounts for approximately 80% of the total matter in the Universe [2]. While DM is widely believed to consist of elementary particles, its mass and interaction properties remain largely unknown [3, 4]. Since the proposal of DM–nucleus scattering as a means to detect Weakly Interacting Massive Particles (WIMPs) [5], direct detection experiments targeting interactions between DM and Standard Model (SM) particles have become a leading approach to probe its nature [6, 7].

In the laboratory frame, DM particles have typical velocities of order 10^{-3} (in units of the speed of light), corresponding to kinetic energies around 10^{-6} times their mass. In elastic scattering processes, the energy transfer is always smaller than the incoming DM energy. As a result, for DM masses above the GeV scale, experimental efforts focus on detecting nuclear recoil signals with keV-scale thresholds [8, 9]. For MeV–GeV DM, detection strategies shift toward eV-scale excitations in crystals or electron scattering [10–15]. For even lighter DM, novel approaches employing ultra-low-threshold platforms, such as cold-atom interferometers or superconducting detectors, have been proposed [16–18].

However, for sub-keV DM, the kinetic energy is below 10^{-3} eV, placing it in a regime where no established experimental technique is currently sensitive to such minuscule energy transfers. Although energy transfer in light DM scattering is suppressed by the target mass, the momentum transfer is not. Moreover, very light (sub-eV) DM exhibits significantly enhanced scattering rates with macroscopic targets due to its high number density and coherent effects [19–21]. Crucially, the cumulative

effect of continuous scattering, namely, the acceleration imparted to the target, emerges as a novel observable, shifting the focus from traditional single-scatter energy deposition [22–25]. Torsion balance experiments with intrinsic geometric asymmetry are particularly sensitive to such DM-induced acceleration signals [21].

In this work, we present the first systematic analysis of multiple state-of-the-art torsion balance experiments, which are designed to test the Equivalence Principle (EP), to constrain interactions between very light DM and nucleons, establishing the most stringent direct detection limits to date in the $(10^{-2}, 1)$ eV mass range.

DARK MATTER-INDUCED ACCELERATION

In the Milky Way, DM particle velocities follow an isotropic Boltzmann distribution. The Solar System orbits the Galactic Center at $v_S \sim 10^{-3}$ [26], creating relative motion with respect to the DM halo. From the Solar System's perspective, the DM fluid flows like a wind, referred to as the *DM wind*. Since Earth's orbital speed around the Sun is much smaller, the DM wind velocity in the laboratory frame can be approximated as $v_\chi \simeq v_S \sim 10^{-3}$, directed opposite to the Solar motion.

Assuming DM interacts with nucleons ($N = n, p$) via a scattering cross-section $\sigma_{\chi N}$, it transfers momentum q during scattering. For very light DM ($m_\chi \lesssim 1$ eV), the scattering is elastic, with $q \simeq m_\chi v_\chi$, comparable to the incident DM momentum. These interactions lead to DM scattering off macroscopic objects, characterized by a total cross-section σ_{tot} . The resulting force from the DM wind, whose flux is $\rho_\chi v_\chi / m_\chi$, with $\rho_\chi \simeq 0.4 \text{ GeV/cm}^3$ the local DM density, is estimated as $F \sim \rho_\chi v_\chi \sigma_{\text{tot}} q / m_\chi$. With m_{tot} being the total mass of a target, this force

^{*}*Corresponding author. Email: matsumoto@ipmu.jp*

[†]*Corresponding author. Email: jie.sheng@sjtu.edu.cn*

[‡]*Corresponding author. Email: chx@sjtu.edu.cn*

[§]*Corresponding author. Email: lin.zhu@hust.edu.cn*

induces an acceleration on the target object as

$$a \sim \frac{1}{m_{\text{tot}} m_{\chi}} \frac{\rho_{\chi}}{m_{\chi}} \sigma_{\text{tot}} v_{\chi} q \simeq \frac{\rho_{\chi} \sigma_{\text{tot}} v_{\chi}^2}{m_{\text{tot}}}. \quad (1)$$

According to the uncertainty principle, the coherent scattering length is defined as $\lambda \equiv 1/q$, where $q \equiv |\mathbf{q}| \sim m_{\chi} v_{\chi} \simeq 10^{-3} m_{\chi}$. Within this coherent length, individual scattering events between the incident particle and constituents of the target become indistinguishable, requiring coherent summation of probability amplitudes. For instance, when λ exceeds the nuclear radius, the DM–nucleus scattering cross-section is enhanced to $\sigma_{\chi A} = A^2 \sigma_{\chi N}$, where A is the atomic mass number. This A^2 enhancement has already been experimentally confirmed in coherent neutrino–nucleus scattering [27].

When $m_{\chi} \lesssim 1$ eV, the coherent scattering length satisfies $\lambda \gtrsim 1 \mu\text{m}$, far exceeding typical interatomic distances. As a result, DM scattering off a macroscopic object must account for interference between different atomic sites, and the total cross-section becomes $\sigma_{\text{tot}} = \sum_{i,j}^{N_A} e^{i\mathbf{q} \cdot \Delta\mathbf{r}_{ij}} \sigma_{\chi A}$ [21]. Here, the displacement between two nuclei is $\Delta\mathbf{r}_{ij} \equiv \mathbf{r}_i - \mathbf{r}_j$, typically of the order of the target size. When the coherence length exceeds the target size, i.e., $1/q \gg |\Delta\mathbf{r}_{ij}|$, the phase factor approaches unity: $e^{i\mathbf{q} \cdot \Delta\mathbf{r}_{ij}} \simeq 1$. In this regime, the total cross-section is enhanced by a factor of N_A^2 , where N_A denotes the number of atoms in the target. For instance, with $m_{\chi} = 10^{-2}$ eV and $\sigma_{\chi A} = 10^{-50} \text{ cm}^2$, the total scattering rate for a macroscopic target with $N_A \sim 10^{24}$ reaches $\sim 10^{16} \text{ s}^{-1}$, resulting in a measurable acceleration,

$$a \simeq 4 \cdot 10^{-12} \text{ cm/s}^2 \times \left(\frac{\sigma_{\chi A}}{10^{-50} \text{ cm}^2} \right) \left(\frac{N_A}{10^{24}} \right). \quad (2)$$

This shows that the DM wind continuously exerts a small force on macroscopic objects, including ourselves.

For a general momentum transfer \mathbf{q} , the sum of phase factors can be expressed via a form factor $F(\mathbf{q})$ as follows:

$$\sum_{i,j=1}^{N_A} e^{i\mathbf{q} \cdot \Delta\mathbf{r}_{ij}} \equiv N_A + (N_A^2 - N_A) |F(\mathbf{q})|^2. \quad (3)$$

In the limit of large atomic number density, the sum in the form factor can be approximated by an integral:

$$|F(\mathbf{q})|^2 = \frac{1}{V^2} \int d^3\mathbf{r}_i d^3\mathbf{r}_j e^{i\mathbf{q} \cdot \Delta\mathbf{r}_{ij}}. \quad (4)$$

Therefore, the total differential cross section for DM scattering off a macroscopic target can be written as:

$$\frac{d\sigma_{\text{tot}}}{d\mathbf{q}} = A^2 [N_A + (N_A^2 - N_A) |F(\mathbf{q})|^2] \frac{d\sigma_{\chi N}}{d\mathbf{q}}, \quad (5)$$

in the weak interaction regime. In contrast, in the strong interaction limit, the total scattering cross section saturates to the geometric size S of the target [19, 20].

Although Eq. (1) provides a qualitative estimate, a full evaluation requires phase-space integration over the anisotropic DM velocity distribution in the laboratory frame, $f(\mathbf{v}_{\chi})$, assuming the z -axis as the detection axis:

$$\langle a_z \rangle = \frac{1}{m_{\text{tot}} m_{\chi}} \frac{\rho_{\chi}}{m_{\chi}} \int d^3\mathbf{v}_{\chi} d\Omega'_{\chi} q_z |\mathbf{v}_{\chi}| f(\mathbf{v}_{\chi}) \frac{d\sigma_{\text{tot}}(\mathbf{q})}{d\Omega'_{\chi}}. \quad (6)$$

Since the initial and final DM momenta share the same magnitude, $m_{\chi} |\mathbf{v}_{\chi}|$, the momentum transfer \mathbf{q} is determined by the scattering angle of the outgoing DM, denoted Ω'_{χ} . Accordingly, the \mathbf{q} -dependence of the differential cross section can be expressed in terms of Ω'_{χ} . The resulting acceleration may be probed by EP-testing torsion balance experiments with asymmetric configurations.

EP-TESTING TORSION BALANCE EXPS

To test the Equivalence Principle, torsion balance experiments often use test bodies made of different materials to probe potential differences in the gravitational-to-inertial mass ratio. Although the test bodies are typically mass-matched, their differing material densities yield distinct volumes and spatial mass distributions. This asymmetry alters the scattering form factor $|F(\mathbf{q})|^2$ between DM and each test body [21], potentially generating measurable differential acceleration signals, $\Delta a \equiv \langle a_z^i \rangle - \langle a_z^j \rangle$, where i and j label the test bodies.

In the following, we discuss several torsion balance experiments, analyzing their form factors and sensitivities to potential DM-induced differential accelerations.

1. **Roll et al. (1964)** [30]: This experiment employed a torsion balance setup with three cylindrical test bodies: two made of aluminum (Al) and one of gold (Au). All cylinders weighed 30 g, but differed in cross-sectional dimensions. The Al cylinders had a base diameter of 2.1 cm and a height of 3.2 cm, while the Au cylinder had a smaller diameter of 0.78 cm but the same height. The test bodies were suspended in an equilateral triangular configuration. As the Earth rotates, the EP-violating acceleration difference toward the Sun varies periodically and becomes detectable. The experiment constrained the acceleration difference between Al and Au to $|\Delta a| < 1.8 \times 10^{-11} \text{ cm/s}^2$ at 95 % confidence level.
2. **Braginskii et al. (1972)** [28]: This experiment employed a torsion pendulum with eight spherical test bodies: four aluminum (Al) and four platinum (Pt). All spheres had equal mass, totaling 3.9 g. The radii of the test bodies were 0.35 cm for Al and 0.18 cm for Pt. As in other setups, the Sun acted as the attractor, and Earth's rotation induced an oscillating EP-violating torque. Despite the use

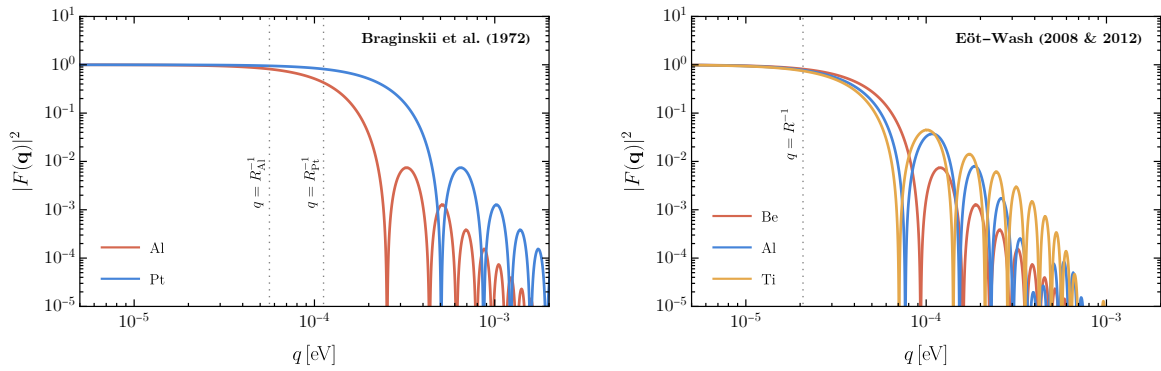


FIG. 1: Form factors of the test bodies used in Braginskii et al. [28] (left) and Eöt-Wash (2008 & 2012) [29] (right). In the former, the radii of the spherical bodies are $R_{\text{Al}} = 0.35 \text{ cm}$ and $R_{\text{Pt}} = 0.18 \text{ cm}$; in the latter, the effective outer radius is $R = 0.95 \text{ cm}$.

of test masses with differing sizes, the experiment achieved improved sensitivity, yielding the bound on the acceleration, $|\Delta a| < 1.1 \times 10^{-12} \text{ cm/s}^2$.

3. **Eöt-Wash (1994) [31–33]:** The Eöt-Wash group developed a rotating torsion balance with a rotation period of approximately 2 h. By modulating the signal at this frequency, low-frequency noise and diurnal backgrounds were effectively suppressed. Due to Earth’s rotation, the suspension fiber was misaligned with the local gravitational vector. As a result, Earth acted as an attractor, exerting EP-violating forces on the test bodies; their horizontal components perpendicular to the fiber induced a measurable torque. The experiment [33] employed two pairs of cylindrical test bodies: beryllium/aluminum (Be/Al) and beryllium/copper (Be/Cu), each with a mass of 10 g. To reduce systematics, all test bodies shared the same outer dimensions—2.0 cm in diameter and 1.7 cm in height. To compensate for density differences, the Be cylinders were solid, while the denser Al and Cu ones were hollow. The resulting limits on EP-violating acceleration were $|\Delta a| < 9.0 \times 10^{-12} \text{ cm/s}^2$ for the Be/Al setup and $|\Delta a| < 1.0 \times 10^{-11} \text{ cm/s}^2$ for Be/Cu.
4. **Eöt-Wash (2008 & 2012) [29, 34]:** These experiments also employed two sets of test bodies: beryllium (Be)/aluminum (Al) and beryllium (Be)/titanium (Ti), each weighing 5 g with identical outer dimensions. Although the test bodies had symmetric yet highly irregular shapes, we approximate them as spheres for this analysis. The Be bodies are modeled as solid spheres with an effective radius of 0.95 cm, while the Al and Ti bodies, sharing the same radius, are treated as spherical shells. A rotating torsion balance was again used, with the Earth serving as the attractor. The experiment achieved sensitivities of $|\Delta a| < 4.7 \times 10^{-13} \text{ cm/s}^2$

for Be/Al and $|\Delta a| < 6.2 \times 10^{-13} \text{ cm/s}^2$ for Be/Ti.

The test bodies used in the above experiments can be classified into four geometries: solid spheres, hollow spheres, solid cylinders, and hollow cylinders. To evaluate the coherent scattering cross sections between DM and these test bodies, the corresponding form factors are needed. For a solid sphere of radius R , the form factor is obtained by integrating Eq. (4) as follows:

$$F_S(\mathbf{q}) = \frac{3}{(qR)^3} [\sin(qR) - qR \cos(qR)]. \quad (7)$$

For a solid cylinder of radius R and height h , the form factor depends on the momentum transfer components parallel (q_h) and perpendicular (q_R) to the cylinder axis,

$$F_C(\mathbf{q}) = \frac{1 - e^{iq_h h}}{iq_h h} \frac{2J_1(q_R R)}{q_R R}. \quad (8)$$

where $J_1(x)$ is the Bessel function of the first kind. A hollow spherical shell or hollow cylinder can be treated as a larger solid shape with a smaller one removed from the center. The form factors for a hollow sphere, $F_{HS}(\mathbf{q})$ and hollow cylinder, $F_{HC}(\mathbf{q})$, can then be derived from those of the corresponding solid shapes,

$$F_{HS,HC}(\mathbf{q}) = \frac{V_{\text{out}} F_{S,C}^{\text{out}}(\mathbf{q}) - V_{\text{in}} F_{S,C}^{\text{in}}(\mathbf{q})}{V_{\text{out}} - V_{\text{in}}}. \quad (9)$$

Here, the labels *out* and *in* refer to the outer and inner dimensions of the test bodies, indicating the corresponding volumes V and form factors F . All form factors approach 1 in the small- \mathbf{q} limit and vanish in the large- \mathbf{q} limit.

The form factors of the test bodies used in the Braginskii et al. (1972) and Eöt-Wash (2008 & 2012) experiments are shown in Fig. 1. Coherent effects are suppressed when the scattering length becomes shorter than the target size, $\lambda \lesssim R$, as expected. In the former experiment, the different radii of the Al and Pt spheres result in notable deviations in their form factors at $q > R_{\text{Al}}^{-1}$.

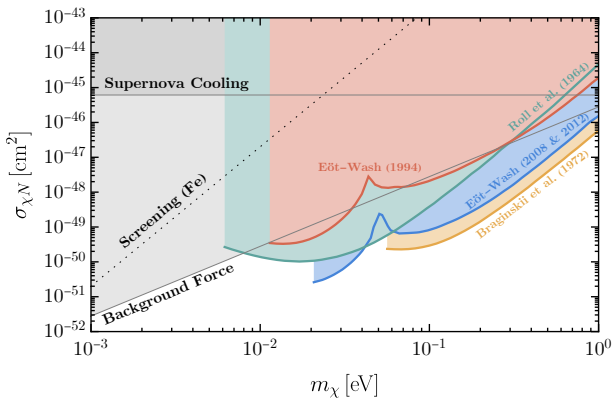


FIG. 2: Constraints on the DM–nucleon cross-section from existing EP tests. The gray shaded regions are excluded by supernova cooling and DM-induced background forces. The dotted curve indicates potential screening by a thick iron wall.

In the latter, where the test bodies share similar outer radii, the form factors only diverge at large q that resolve their internal hollowness, with the magnitude of the difference much smaller than in the case of distinct outer dimensions.

CONSTRAINTS

When the DM scattering is isotropic, $d\sigma_{\chi N}/d\Omega'_\chi = \sigma_{\chi N}/4\pi$, the differences in the scattering cross sections among test bodies in Eq. (6) arise solely from their form factors. These form factor differences induce differential accelerations via coherent DM scattering in EP-testing experiments. The null results from such tests constrain the cross section $\sigma_{\chi N}$, i.e., DM interaction with nucleons. The resulting limits from the above experiments are shown in Fig. 2. The strongest sensitivity is attained when the DM de Broglie wavelength is comparable to the test body size. For heavier DM, coherence is lost, weakening the constraint. For lighter DM, the de Broglie wavelength exceeds the size of the experimental apparatus, rendering the definition of an individual-body cross section ill-posed and invalidating the present analysis.

If the DM interaction is sufficiently strong, screening effects inside matter can become significant [25, 35, 36]. Given the DM–nucleon coupling $\mathcal{L} = -\chi^2 \bar{N} N/(2f)$, DM acquires an effective mass in materials. If this effective mass is large, the DM wind is exponentially suppressed within matter and thus screened. The region in which a sufficiently thick iron wall screens the DM wind is indicated by the dotted curve in Fig. 2. However, this constraint does not apply if the DM–nucleon potential is attractive. See Appendix A for further details.

DM within the same mass range is subject to other indirect constraints. First, the same coupling leads to DM production in supernovae via nucleon bremsstrahlung,

$N+N \rightarrow N+N+\chi+\chi$, thereby affecting supernova cooling. Observations require that the emission of light DM not significantly exceed that of neutrinos [37]. The corresponding constraints [38] are shown as the shaded gray region in Fig. 2. Additionally, quadratically coupled DM can induce forces between nucleons [39–43]. When a DM wave scatters off a source nucleon, it modifies the effective mass of a nearby test nucleon, which then experiences a force proportional to the gradient of this mass. The resulting constraint [39] from short-range EP tests [44] appears as the light gray shaded region in Fig. 2.

DISCUSSION AND CONCLUSIONS

In this paper, we have shown that although detecting single scattering events from light DM is challenging due to limited energy transfer, the acceleration of macroscopic objects caused by continuous scattering may offer a novel observable. Coherent scattering significantly enhances both the cross-section and the resulting acceleration signal. Such effects are measurable using torsion balance experiments with asymmetric configurations. We systematically analyzed several state-of-the-art torsion balance setups originally developed for weak equivalence principle tests, deriving constraints on DM–nucleon scattering across the mass range $(10^{-2}, 1)$ eV. Compared to existing bounds, torsion balance experiments exhibit superior sensitivity. This opens a new avenue for direct detection of low-mass DM. Enhancing the asymmetry in torsion balance configurations could further probe weaker DM–nucleon couplings. A proposed rotating torsion balance with test bodies of differing outer dimensions offers improved sensitivity to coherent DM scattering [21].

Acknowledgements

The authors thank Peter Cox, Shao-Feng Ge, Peng-Shun Luo, and Yevgeny Stadnik for fruitful discussions. S. M. was supported by the Grant-in-Aid for Scientific Research from the Ministry of Education, Culture, Sports, Science and Technology, Japan (MEXT), under Grant No. 24H00244. J. S. is supported by the National Natural Science Foundation of China (Nos. 12375101, 12425506, 12090060, 12090064) and the SJTU Double First Class start-up fund WF220442604. C.-Y. Xing is supported by the Fundamental Research Funds for the Central Universities (No. 24CX06048A). L. Zhu is supported by the National Natural Science Foundation of China (No. 12005308 and No. 12150012).

Appendix A – Screening Effects

The coupling between DM (ϕ) and nucleons is given by

$$\mathcal{L} = \pm \frac{1}{2f} \phi^2 \bar{N} N, \quad (10)$$

where the positive (negative) sign corresponds to an attractive (repulsive) potential between DM and nucleons. Here, we discuss in detail how such interactions influence the screening effects of DM in experiments.

Repulsive Potential – The interaction Lagrangian, $\mathcal{L} = -\phi^2 \bar{N} N / 2f$, effectively behaves as a DM mass term when the nucleon field acquires an expectation value $\langle \bar{N} N \rangle = n_N$ in matter, with n_N denoting the nucleon number density. Then, DM acquires an effective mass,

$$\Delta m_\phi^2 = \frac{1}{f} \langle \bar{N} N \rangle = \frac{n_N}{f}, \quad (11)$$

When DM with mass m_χ and momentum \mathbf{p}_χ enters a material medium from vacuum, the dispersion relation

$$\sqrt{\mathbf{p}_\chi'^2 + m_\chi^2 + \Delta m_\phi^2} = \sqrt{\mathbf{p}_\chi^2 + m_\chi^2}, \quad (12)$$

dictates that the DM momentum inside matter \mathbf{p}'_χ is,

$$|\mathbf{p}'_\chi| = \sqrt{\mathbf{p}_\chi^2 - \Delta m_\phi^2}. \quad (13)$$

If the coupling is strong enough that the DM effective mass exceeds its vacuum momentum, $\Delta m_\phi > |\mathbf{p}_\chi|$, the DM momentum inside the material becomes imaginary. This implies that the DM wave is exponentially attenuated while passing through the material. When the material thickness exceeds the DM penetration depth, the wave is fully reflected, resulting in a *screening effect*. Only when $\Delta m_\phi < |\mathbf{p}_\chi|$ can DM propagate through the material. In the main text (and in Fig. 2), we adopt this as the condition for DM to remain unshielded.

For the experiments under consideration, potential sources of DM shielding include the Earth's atmosphere and the external shield of the torsion balance apparatus. The mass density of the atmosphere near sea level is observed to be $\rho_{\text{atmo}} \sim 0.0012 \text{ g/cm}^3$, corresponding to a nuclear number density of $n_{\text{atmo}} \simeq \rho_{\text{atmo}} / 1 \text{ GeV}$. To ensure that DM is not significantly attenuated in the atmosphere, the following condition must be satisfied:

$$f \gtrsim \frac{n_{\text{atmo}}}{m_\phi^2 v_\phi^2} \sim 5 \cdot 10^7 \times \left(\frac{m_\phi}{10^{-2} \text{ eV}} \right)^{-2} \text{ GeV}. \quad (14)$$

Translated to the scattering cross-section, this becomes,

$$\sigma_{\chi N} \lesssim 6 \cdot 10^{-40} \times \left(\frac{m_\phi}{10^{-2} \text{ eV}} \right)^4 \text{ cm}^2. \quad (15)$$

Assuming the torsion balance apparatus is encased in a shield, the condition for DM to remain unshielded is

a thick iron layer with density $\rho_{\text{Fe}} \sim 7.87 \text{ g/cm}^3$ (other materials would not significantly affect the result), the condition for DM to penetrate the shield is:

$$\sigma_{\chi N} \lesssim 2 \cdot 10^{-47} \times \left(\frac{m_\phi}{10^{-2} \text{ eV}} \right)^4 \text{ cm}^2. \quad (16)$$

Due to iron's higher nuclear number density, it imposes stronger constraints on the cross-section. In Fig. 2, the condition in Eq. (16) is shown as a black dotted line. For DM-nucleon interactions with a repulsive potential, the parameter space above this line may be shielded.

Reference [25] describes the modification of the DM effective mass due to interactions as a Meissner-like effect. Essentially, this is analogous to the quantum mechanical scattering of a particle by a potential barrier: when the barrier height exceeds the particle's kinetic energy, the transmission amplitude is exponentially suppressed.

Attractive Potential – The positive interacting Lagrangian, $\mathcal{L} = +\phi^2 \bar{N} N / (2f)$, represents an attractive potential between DM and nucleons. It induces a negative effective mass-squared term for the DM field, $\Delta m_\phi^2 = -n_N/f$. In this case, the dispersion relation becomes

$$\sqrt{\mathbf{p}_\chi'^2 + m_\chi^2 - |\Delta m_\phi^2|} = \sqrt{\mathbf{p}_\chi^2 + m_\chi^2}, \quad (17)$$

dictating that the DM momentum inside matter,

$$|\mathbf{p}'_\chi| = \sqrt{\mathbf{p}_\chi^2 + |\Delta m_\phi^2|} \quad (18)$$

is always positive. This implies that DM can still propagate inside matter. Consequently, when DM–nucleon interactions are attractive, no screening effect arises, and the constraints shown in Fig. 2 become irrelevant.

* Electronic address: shigeki.matsumoto@ipmu.jp

† Electronic address: shengjie04@sjtu.edu.cn

‡ Electronic address: cyxing@upc.edu.cn

§ Electronic address: zhulin36@mail.hust.edu.cn

- [1] B.-L. Young, “*A survey of dark matter and related topics in cosmology*,” *Front. Phys. (Beijing)* **12** no. 2, (2017) 121201. [Erratum: *Front.Phys.(Beijing)* 12, 121202 (2017)].
- [2] **Planck** Collaboration, N. Aghanim *et al.*, “*Planck 2018 results. VI. Cosmological parameters*,” *Astron. Astrophys.* **641** (2020) A6, [[arXiv:1807.06209](https://arxiv.org/abs/1807.06209) [astro-ph.CO]]. [Erratum: *Astron.Astrophys.* 652, C4 (2021)].
- [3] G. Bertone, D. Hooper, and J. Silk, “*Particle dark matter: Evidence, candidates and constraints*,” *Phys. Rept.* **405** (2005) 279–390, [[arXiv:hep-ph/0404175](https://arxiv.org/abs/hep-ph/0404175)].
- [4] A. Arbey and F. Mahmoudi, “*Dark matter and the early Universe: a review*,” *Prog. Part. Nucl. Phys.* **119** (2021) 103865, [[arXiv:2104.11488](https://arxiv.org/abs/2104.11488) [hep-ph]].
- [5] M. W. Goodman and E. Witten, “*Detectability of Certain Dark Matter Candidates*,” *Phys. Rev. D* **31** (1985) 3059.

[6] T. Lin, “*Dark matter models and direct detection*,” *PoS* **333** (2019) 009, [[arXiv:1904.07915](#) [hep-ph]].

[7] J. Cooley, “*Dark Matter direct detection of classical WIMPs*,” *SciPost Phys. Lect. Notes* **55** (2022) 1, [[arXiv:2110.02359](#) [hep-ph]].

[8] J. Billard *et al.*, “*Direct detection of dark matter—APPEC committee report**,” *Rept. Prog. Phys.* **85** no. 5, (2022) 056201, [[arXiv:2104.07634](#) [hep-ex]].

[9] D. S. Akerib *et al.*, “*Snowmass2021 Cosmic Frontier Dark Matter Direct Detection to the Neutrino Fog*,” in *Snowmass 2021*. 3, 2022. [[arXiv:2203.08084](#) [hep-ex]].

[10] R. Essig, J. Mardon, and T. Volansky, “*Direct Detection of Sub-GeV Dark Matter*,” *Phys. Rev. D* **85** (2012) 076007, [[arXiv:1108.5383](#) [hep-ph]].

[11] S. Knapen, T. Lin, M. Pyle, and K. M. Zurek, “*Detection of Light Dark Matter With Optical Phonons in Polar Materials*,” *Phys. Lett. B* **785** (2018) 386–390, [[arXiv:1712.06598](#) [hep-ph]].

[12] S. Griffin, S. Knapen, T. Lin, and K. M. Zurek, “*Directional Detection of Light Dark Matter with Polar Materials*,” *Phys. Rev. D* **98** no. 11, (2018) 115034, [[arXiv:1807.10291](#) [hep-ph]].

[13] A. Coskuner, T. Trickle, Z. Zhang, and K. M. Zurek, “*Directional detectability of dark matter with single phonon excitations: Target comparison*,” *Phys. Rev. D* **105** no. 1, (2022) 015010, [[arXiv:2102.09567](#) [hep-ph]].

[14] B. Campbell-Deem, S. Knapen, T. Lin, and E. Villarama, “*Dark matter direct detection from the single phonon to the nuclear recoil regime*,” *Phys. Rev. D* **106** no. 3, (2022) 036019, [[arXiv:2205.02250](#) [hep-ph]].

[15] A. Mitridate, T. Trickle, Z. Zhang, and K. M. Zurek, “*Snowmass white paper: Light dark matter direct detection at the interface with condensed matter physics*,” *Phys. Dark Univ.* **40** (2023) 101221, [[arXiv:2203.07492](#) [hep-ph]].

[16] G. Afek, D. Carney, and D. C. Moore, “*Coherent Scattering of Low Mass Dark Matter from Optically Trapped Sensors*,” *Phys. Rev. Lett.* **128** no. 10, (2022) 101301, [[arXiv:2111.03597](#) [physics.ins-det]].

[17] R. Essig *et al.*, “*Snowmass2021 Cosmic Frontier: The landscape of low-threshold dark matter direct detection in the next decade*,” in *Snowmass 2021*. 3, 2022. [[arXiv:2203.08297](#) [hep-ph]].

[18] C. G. Baker, W. P. Bowen, P. Cox, M. J. Dolan, M. Goryachev, and G. Harris, “*Optomechanical dark matter instrument for direct detection*,” *Phys. Rev. D* **110** no. 4, (2024) 043005, [[arXiv:2306.09726](#) [hep-ph]].

[19] H. Fukuda, S. Matsumoto, and T. T. Yanagida, “*Direct Detection of Ultralight Dark Matter via Astronomical Ephemeris*,” *Phys. Lett. B* **789** (2019) 220–227, [[arXiv:1801.02807](#) [hep-ph]].

[20] H. Fukuda and S. Shirai, “*Detection of QCD axion dark matter by coherent scattering*,” *Phys. Rev. D* **105** no. 9, (2022) 095030, [[arXiv:2112.13536](#) [hep-ph]].

[21] P. Luo, S. Matsumoto, J. Sheng, C.-Y. Xing, L. Zhu, and Z.-J. Zhuge, “*Detecting meV-Scale Dark Matter via Coherent Scattering with an Asymmetric Torsion Balance*,” [[arXiv:2409.09950](#) [hep-ph]].

[22] V. Domcke and M. Spinrath, “*Detection prospects for the Cosmic Neutrino Background using laser interferometers*,” *JCAP* **06** (2017) 055, [[arXiv:1703.08629](#) [astro-ph.CO]].

[23] P. W. Graham, D. E. Kaplan, J. Mardon, S. Rajendran, and W. A. Terrano, “*Dark Matter Direct Detection with Accelerometers*,” *Phys. Rev. D* **93** no. 7, (2016) 075029, [[arXiv:1512.06165](#) [hep-ph]].

[24] D. Carney, A. Hook, Z. Liu, J. M. Taylor, and Y. Zhao, “*Ultralight dark matter detection with mechanical quantum sensors*,” *New J. Phys.* **23** no. 2, (2021) 023041, [[arXiv:1908.04797](#) [hep-ph]].

[25] H. Day, D. Liu, M. A. Luty, and Y. Zhao, “*Blowing in the Dark Matter Wind*,” [[arXiv:2312.13345](#) [hep-ph]].

[26] D. Baxter *et al.*, “*Recommended conventions for reporting results from direct dark matter searches*,” *Eur. Phys. J. C* **81** no. 10, (2021) 907, [[arXiv:2105.00599](#) [hep-ex]].

[27] **COHERENT** Collaboration, D. Akimov *et al.*, “*Observation of Coherent Elastic Neutrino-Nucleus Scattering*,” *Science* **357** no. 6356, (2017) 1123–1126, [[arXiv:1708.01294](#) [nucl-ex]].

[28] V. B. Braginskii and V. I. Panov, “*Verification of equivalence of inertial and gravitational masses*,” *Sov. Phys. JETP* **34** (1972) 463–476.

[29] T. A. Wagner, S. Schlamminger, J. H. Gundlach, and E. G. Adelberger, “*Torsion-balance tests of the weak equivalence principle*,” *Class. Quant. Grav.* **29** (2012) 184002, [[arXiv:1207.2442](#) [gr-qc]].

[30] P. G. Roll, R. Krotkov, and R. H. Dicke, “*The Equivalence of inertial and passive gravitational mass*,” *Annals Phys.* **26** (1964) 442–517.

[31] B. R. Heckel, E. G. Adelberger, C. W. Stubbs, Y. Su, H. E. Swanson, G. Smith, and W. F. Rogers, “*EXPERIMENTAL BOUNDS ON INTERACTIONS MEDIATED BY ULTRALOW MASS BOSONS*,” *Phys. Rev. Lett.* **63** (1989) 2705–2708.

[32] E. G. Adelberger, C. W. Stubbs, B. R. Heckel, Y. Su, H. E. Swanson, G. Smith, J. H. Gundlach, and W. F. Rogers, “*Testing the equivalence principle in the field of the earth: Particle physics at masses below 1-microEV?*,” *Phys. Rev. D* **42** (1990) 3267–3292.

[33] Y. Su, B. R. Heckel, E. G. Adelberger, J. H. Gundlach, M. Harris, G. L. Smith, and H. E. Swanson, “*New tests of the universality of free fall*,” *Phys. Rev. D* **50** (1994) 3614–3636.

[34] S. Schlamminger, K. Y. Choi, T. A. Wagner, J. H. Gundlach, and E. G. Adelberger, “*Test of the equivalence principle using a rotating torsion balance*,” *Phys. Rev. Lett.* **100** (2008) 041101, [[arXiv:0712.0607](#) [gr-qc]].

[35] A. Hees, O. Minazzoli, E. Savalle, Y. V. Stadnik, and P. Wolf, “*Violation of the equivalence principle from light scalar dark matter*,” *Phys. Rev. D* **98** no. 6, (2018) 064051, [[arXiv:1807.04512](#) [gr-qc]].

[36] A. Banerjee, G. Perez, M. Safronova, I. Savoray, and A. Shalit, “*The phenomenology of quadratically coupled ultra light dark matter*,” *JHEP* **10** (2023) 042, [[arXiv:2211.05174](#) [hep-ph]].

[37] G. G. Raffelt, *Stars as laboratories for fundamental physics: The astrophysics of neutrinos, axions, and other weakly interacting particles*. 5, 1996.

[38] K. A. Olive and M. Pospelov, “*Environmental dependence of masses and coupling constants*,” *Phys. Rev. D* **77** (2008) 043524, [[arXiv:0709.3825](#) [hep-ph]].

[39] K. Van Tilburg, “*Wake forces in a background of quadratically coupled mediators*,” *Phys. Rev. D* **109** no. 9, (2024) 096036, [[arXiv:2401.08745](#) [hep-ph]].

[40] S. Barbosa and S. Fichet, “*Background-induced forces*

from dark relics,” *JHEP* **01** (2025) 021, [[arXiv:2403.13894](https://arxiv.org/abs/2403.13894) [hep-ph]].

[41] Y. Grossman, B. Yu, and S. Zhou, “Axion forces in axion backgrounds,” [[arXiv:2504.00104](https://arxiv.org/abs/2504.00104) [hep-ph]].

[42] Y. Cheng and S. Ge, “Background-Enhanced Axion Force by Axion Dark Matter,” [[arXiv:2504.02702](https://arxiv.org/abs/2504.02702) [hep-ph]].

[43] X. Gan, D. Liu, D. Liu, X. Luo, and B. Yu, “Detecting Ultralight Dark Matter with Matter Effect,” [[arXiv:2504.11522](https://arxiv.org/abs/2504.11522) [hep-ph]].

[44] W.-H. Tan *et al.*, “Improvement for Testing the Gravitational Inverse-Square Law at the Submillimeter Range,” *Phys. Rev. Lett.* **124** no. 5, (2020) 051301.